IEEE Access
Multidisciplinary | Rapid Review | Open Access Journal

Received December 21, 2018, accepted December 25, 2018, date of publication January 14, 2019, date of current version February 6, 2019.

*Digital Object Identifier 10.1109/ACCESS.2019.2892711*

# Analysis of a Packable and Tunable Origami Multi-Radii Helical Antenna

**XUELI LIU, (Student Member, IEEE), CONSTANTINOS L. ZEKIOS, (Member, IEEE), AND STAVROS V. GEORGAKOPOULOS, (Senior Member, IEEE)**
Department of Electrical and Computer Engineering, Florida International University, Miami, FL 33174, USA

Corresponding author: Stavros V. Georgakopoulos (georgako@fiu.edu))

This work was supported in part by the National Science Foundation under Grant EFRI 1332348, in part by the Air Force Office of Scientific Research under Grant FA9550-18-1-0191, and in part by the 2017-2018 Dissertation Year Fellowship from the UGS of Florida International University.

**ABSTRACT** This paper presents the design process of a multi-radii monofilar helical antenna that can operate in three different bands with circular polarization. The antenna is comprised of two helical antennas with different radii that are embedded and supported by an innovative structural technique. This allows reconfigurable behavior, efficient folding, packaging, and deployment. The antenna is fabricated using 2-mil-thick-FPC Kapton with a 3-mil copper trace glued appropriately on the top. An actuation mechanism of telescopic form is used for the stress-free deployment of the proposed design. The proposed origami antenna can adjust its band of operation by changing its height; therefore, it is physically reconfigurable. The main advantage of this antenna is that it can cover multiple applications, such as GPS, WiMAX, and satellite radio communications with a measured maximum right-hand circularly polarized realized gain of 6.3, 12.7, and 10.5 dB, respectively, thereby eliminating the need for multiple antennas.

**INDEX TERMS** Circular polarization, origami, reconfigurable, multi-radii helix.

## I. INTRODUCTION

Deployable antennas have been recently developed [1]–[4] exhibiting unique advantages of reconfigurability and collapsibility. Their concept of design is based on the origami idea, an advantageous technique, since the 3D geometry can be made by first using standard planar manufacturing to create the planar geometry of the antenna and then fold it into the 3D structure, [6]–[9].

The trend of origami based electromagnetic (EM) structures has been significantly grown the last 5 years. The Nojima wrap antenna, [1], and the Nejiri cylinder antenna, [2], are some examples of designs that can change their geometries while operating, thereby reconfiguring their electromagnetic performance. In this paper, a multi-radii helical antenna is analyzed following the design approach published in [2].

Helical antennas have been thoroughly analyzed and studied [10]–[17]. Various designs have been introduced [1]–[17], [22], [23], operating in axial mode, which makes them suitable for satellite applications. Recently, the increased interest for deployable antennas led to the design of a new type of helical based antennas. Specifically, a deployable quadrifilar helix antenna and a conical log spiral antenna were proposed for the UHF band in [3]. Also, a conical log spiral antenna for WiMAX applications in the range of 2.2 GHz to 3 GHz was proposed in [4]. For both cases the designs operate with high efficiency within the band of interest. In this paper, the design methodology for our helical antenna is different from the ones presented previously. Our origami multi-radii helical antenna can change its height to tune its operating frequency to different frequency bands to satisfy different requirements. The introduction of more than one helical sections is found to be critical for improving the bandwidth of the gain, pattern, and circular-polarization, which agrees with [18]. Here, for the first time, a multi-radii helical antenna is designed so that it can morph its shape to provide optimal tunable bandwidth and packing. The proposed antenna can cover three bands of operation, namely, GPS, WiMAX and Satellite Radio communications and achieve a measured maximum RHCP realized gain of 6.3 dB, 12.7 dB and 10.5 dB, respectively. Also, its axial ratio remains below 2 dB for all the three bands.

## II. MULTI-RADII HELICAL ANTENNA ORIGAMI DESIGN

The proposed reconfigurable multi-radii helix consists of two helical sections (a top and a bottom one) with different radii and a transition step between them to serially connect the

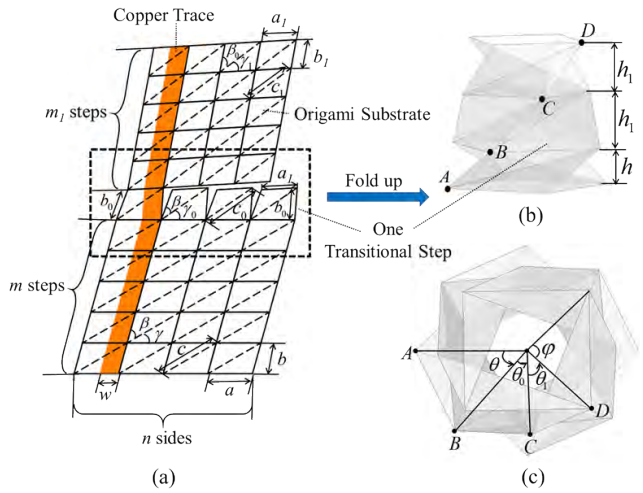


**FIGURE 1.** Geometries of the origami multi-radii monofilar helix: (a) origami folding pattern, (b) perspective view of multi-radii folded-up transition section, and (c) top view of multi-radii folded-up transition section.

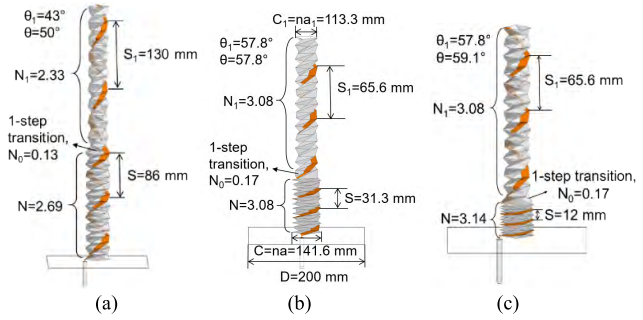


**FIGURE 2.** Models and geometries of the origami multi-radii helix at three different heights (i.e., states): (a) state 1 (unfolded state), (b) state 2 (semi-folded state), and (c) state 3 (folded state).

two helical sections, as shown in Figs. 1 and 2. The proposed origami pattern for folding a multi-radii origami cylindrical base is shown in Fig. 1(a). Only a few dominant parameters need to be determined, i.e., *a, ratio,* $f_{scale}$, $ratio_1$, $m_1$, *m, n* and *w*, whose designed values and descriptions are listed in TABLE 1. By folding along the hills and valleys in Fig. 1(a) as denoted by solid and dash lines, respectively, combining the bottom and top sections and connecting the left and right side of the origami pattern, the entire origami base is folded up. Two other dominant parameters in the 3-D folded-up origami base are $\theta$ and $\theta_1$ as denoted in Fig. 1(c) and explained in TABLE 1. Specifically, $\theta$ and $\theta_1$ are variables and control the height of each step in the origami base, $h$ and $h_1$, as shown in Fig. 1(b). The heights, $h$ and $h_1$, can be calculated using the formulas shown in TABLE 6. The lengths of the diagonal lines (i.e., $c$, $c_1$ and $c_0$) and the side length $b_0$ of the transition step in Fig. 1(a) are not constant due to the varying $\theta$ and $\theta_1$. Therefore, the substrate used to build the origami base should be stretchable along these hinges besides being foldable; also, internal strains exist near these hinges. The angles in the transition step (i.e., $\beta_0$ and $\gamma_0$) denoted in Fig. 1(a) are also not constant due to the varying side lengths. Therefore, this origami pattern is not rigidly foldable [21].

**TABLE 1.** Primary geometric parameters of origami pattern.

| Dominant Parameter | Description | Designed Value |
|---|---|---|
| $n$ | # of sides of the intersectional polygon | 4 |
| $a$ | Horizontal length of each parallelogram unit in the bottom cylinder | 35.4 *mm* |
| $ratio$ | Length ratio of the vertical and horizontal lengths of each parallelogram unit in the bottom cylinder | 0.7 |
| $m$ | # of steps of the bottom helix | 18 |
| $f_{scale}$ | Ratio of the radius of the top helix to the radius of the bottom helix | 0.8 |
| $ratio_1$ | Length ratio of the vertical and horizontal lengths of each parallelogram unit in the top cylinder | 0.79 |
| $m_1$ | # of steps of the top helix | 18 |
| $w$ | Width of the copper trace | 15 *mm* |
| $\theta$ | Folding angle between adjacent intersectional polygonal planes on the bottom cylinder | Not const. |
| $\theta_1$ | Folding angle between adjacent intersectional polygonal planes on the top cylinder | Not const. |

## III. ANTENNA MODEL DESIGN

The proposed reconfigurable multi-radii origami helix at three reconfigurable states of height is shown in Fig. 2. The pitch sizes of the bottom and top helices, $S$ and $S_1$, can be solely determined by *ratio* and $ratio_1$, respectively, as defined in (1) and (2). Also, the number of turns of the bottom and top helices, $N$ and $N_1$, can be optimized independently solely by changing, $m_1$ and $m$, respectively, without changing the values of the other primary geometric parameters, as expressed below in (3) and (4).

$$S = n \cdot a \sqrt{\frac{ratio^2 \cdot \sin^2\left(\frac{\varphi}{2}\right)}{\sin^2\left(\frac{\theta}{2}\right)} - 1} \tag{1}$$

$$S_1 = na \cdot f_{scale} \sqrt{\frac{ratio_1^2 \cdot \sin^2\left(\frac{\varphi}{2}\right)}{\sin^2\left(\frac{\theta_1}{2}\right)} - 1} \tag{2}$$

$$N = m \cdot \sin\left(\frac{\theta}{2}\right) \Big/ \left[n \cdot \sin\left(\frac{\varphi}{2}\right)\right] \tag{3}$$

$$N_1 = m_1 \cdot \sin\left(\frac{\theta_1}{2}\right) \Big/ \left[n \cdot \sin\left(\frac{\varphi}{2}\right)\right] \tag{4}$$

Note that the number of turns $N_0$ and height $h_1$ of the transition step do not significantly impact the antenna's performance, and $N_0$ is calculated as:

$$N_0 = \sin\left(\frac{\theta_1}{2}\right) \Big/ \left[n \cdot \sin\left(\frac{\varphi}{2}\right)\right] \tag{5}$$

Therefore, the geometries of the two helices can be optimized in terms of the axial ratio (AR) and the 2-dB RHCP realized gain bandwidth by varying the geometric parameters of the origami pattern (i.e., *ratio,* $ratio_1$, *m* and $m_1$). A detailed design process for this antenna is presented in Section IV. The circumferences of both the bottom and top

helices, $C$ and $C_1$, remain approximately constant for different heights (i.e., states of the antenna), as shown in Fig. 2. Also, the total length of the antenna trace $L_{total} = mb + b_0 + m_1 b_1$ remains approximately constant at the 3 states.

According to antenna theory [19] and previous analysis on the axial-mode of origami helical antenna type [2], the pitch size, $S$, circumference, $C$, and pitch angle, $\alpha$, of a broadband single-radius origami helical antenna should satisfy the following conditions in order to achieve optimal performance:

$$S \approx \frac{\lambda_0}{4} \tag{6}$$

$$\frac{3}{4}\lambda_0 < C < \frac{4}{3}\lambda_0 \tag{7}$$

$$12^\circ < \alpha < 14^\circ \tag{8}$$

where,

$$\alpha = \tan^{-1}\frac{h}{\sqrt{b^2 - h^2}} = \tan^{-1}\sqrt{\frac{ratio^2 \cdot \sin^2\left(\frac{\varphi}{2}\right)}{\sin^2\left(\frac{\theta}{2}\right)} - 1} \tag{9}$$

Also, the sense of the circular polarization is determined by the winding direction of the helical trace from its feeding point. The proposed multi-radii origami helix is designed to be right-hand circularly polarized (RHCP).

The proposed helical antenna due to the origami design and the developed actuation system (see Section VII) is collapsible. By appropriately changing the height of the helical antenna, it is able to tune its behavior in terms of frequency, axial ratio and gain. However, when a single-radius origami helical antenna of same size changes its height to tune its performance, its gain and bandwidth decrease and its circular polarization (CP) cannot be maintained (see results in Section VI.B).

Therefore, to address this problem and to improve RHCP gain, radiation pattern, 2-dB realized RHCP gain bandwidth and CP performance at all three states of operation, a second helix with different radius is added on top of the single origami helix [18]. The geometric details of the proposed multi-radii origami helix are tabulated in TABLE 1 and 2 and shown in Fig. 2. In the next section the design process of the origami multi-radii helix is presented.

## IV. DESIGN PROCESS OF THE MULTI-RADII HELICAL ANTENNA

In this section the design process of determining the multi-radii antenna parameters is presented. Only the state 2 is presented for brevity, whilst at other states the parameters are defined following a similar process. The most critical parameters are the circumferences of both helices. The circumference of the bottom helix determines the operational bandwidth, while the circumference of the top helix improves the AR and the RHCP gain. Since the antenna has to operate at the frequency band 1.48 GHz-4.00 GHz (for GPS, WiMAX and Satellite Radio communications), the horizontal length of each parallelogram unit (see Fig. 1), $a$, is determined using (10) as 35.4 mm.

**TABLE 2. Secondary geometric parameters of origami base.**

| Successive Parameter | Calculation | Value |
|---|---|---|
| $\varphi$ | $\varphi = 2\pi/n$ | 90° |
| $\beta$ | $\beta = \pi/n$ [20] | 45° |
| $\gamma$ | $\gamma = \sin^{-1}(ratio \cdot \sin\beta)$ [2] | 29.7° |
| $b$ | $b = ratio \cdot a$ [2] | 24.8 *mm* |
| $c$ | $c = a\sqrt{ratio^2 + \cos\theta + \frac{\sin\theta\sin\varphi}{1-\cos\varphi}}$ | Not const. |
| $b_0$ | $b_0 = a\sqrt{f_{scale}^2 ratio^2 + \frac{f_{scale}^2(\cos\theta_1 - 0.5) - f_{scale}\cos\theta_1 + 0.5}{1-\cos\varphi}}$ | Not const. |
| $c_0$ | $c_0 = a\sqrt{f_{scale}^2 ratio^2 + \frac{f_{scale}^2(\cos\theta_1 - 0.5) - 0.5 f_{scale}\cos(\varphi+\theta_1) + 0.5}{1-\cos\varphi}}$ | Not const. |
| $\beta_0$ | $\beta_0 = \cos^{-1}\left(\frac{b_0^2 + c_0^2 - a_1^2}{2b_0c_0}\right)$ | Not const. |
| $\gamma_0$ | $\gamma_0 = \cos^{-1}\left(\frac{c_0^2 + a^2 - b_0^2}{2ac_0}\right)$ | Not const. |
| $\gamma_1$ | $\gamma = \sin^{-1}(ratio_1 \cdot \sin\beta)$ | 34° |
| $a_1$ | $a_1 = f_{scale} \cdot a$ | 28.3 *mm* |
| $b_1$ | $b_1 = ratio_1 \cdot a_1$ | 22.4 *mm* |
| $c_1$ | $c = a_1\sqrt{ratio_1^2 + \cos\theta_1 + \frac{\sin\theta_1\sin\varphi}{1-\cos\varphi}}$ | Not const. |
| $h$ | $h = a\sqrt{ratio^2 - \frac{\sin^2\left(\frac{\theta}{2}\right)}{\sin^2(\beta)}}$ [2] | Not const. |
| $h_1$ | $h_1 = a_1\sqrt{ratio_1^2 - \frac{\sin^2\left(\frac{\theta_1}{2}\right)}{\sin^2(\beta)}}$ [2] | Not const. |

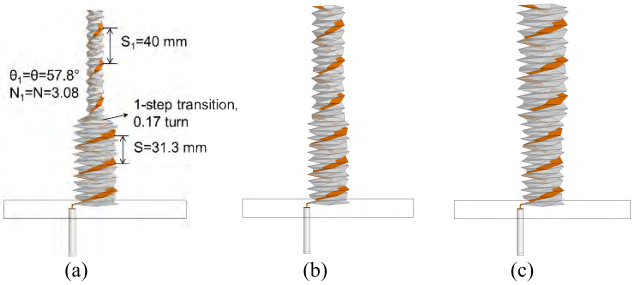


**FIGURE 3. Models of multi-radii helix with variable $f_{scale}$. (a) $f_{scale}$ = 0.4. (b) $f_{scale}$ = 0.8. (c) $f_{scale}$ = 1.2.**

### A. DETERMINING PARAMETER $a_1$ OF THE TOP HELIX

The horizontal length $a_1$ (see Fig. 1) is optimized by varying the dominant parameter $f_{scale}$ as defined in TABLE 1. The $ratio_1$ is evaluated based on (2) and the pitch size of the top helix $S_1$ and bottom helix $S$, are kept constant to the values 40 *mm* and 31.3 *mm*, respectively, which will be optimized later on. The folding angles between adjacent intersectional polygonal planes for both cylinders are set to 57.8° and the number of turns equal to 3.08 using (3), (4). Aiming for a minimum axial ratio and a maximum RHCP gain the value $f_{scale} = 0.8$ is selected after an optimization process. Fig. 3 shows how the multi-radii geometry is modified for different values of $f_{scale}$, while in TABLE 3 the corresponding

**TABLE 3.** Simulated antenna performances vs $f_{scale}$ and $\alpha_1$.

| $f_{scale}$ | $\alpha_1$ | Bandwidth with -2 dB RHCP Gain Variation from the Maximum | Max. RHCP Gain | AR Range |
|---|---|---|---|---|
| 0.4 | 14.2 *mm* | 1.94 GHz-3.52 GHz (Δf=57.9%) | 11.4 dB | 0.4 dB-2.9 dB |
| 0.8 | 28.3 *mm* | 2 GHz-3.52 GHz (Δf=55.1%) | 13.2 dB | 0 dB-2.1 dB |
| 1.2 | 42.4 *mm* | 1.64 GHz-2.72 GHz (Δf=49.5%) | 13 dB | 0.1 dB-2.9 dB |

maximum RHCP gain and AR range is tabulated. It is important to note at this point, based on the results of Table 3, that as $f_{scale}$ increased the 2-dB bandwidth increases, but when it becomes larger than 1, it starts decreasing and the operating frequency band of the antenna shifts to lower frequencies.

### B. DETERMINING THE NUMBER OF TURNS OF THE LARGE HELIX

The number of turns of the large helix, $N$, is optimized aiming for the optimum 2-dB RHCP gain BW. To vary $N$, we vary the number of steps of the large helix, $m$, while maintaining constant $\theta$ and $n$, as shown in (3). The optimum 2-dB RHCP gain bandwidth is achieved for $m = 18$, for the range 1.94 GHz-3.46 GHz, a maximum RHCP gain of 12.7 dB and an AR range of 0.4 dB-3 dB.

### C. DETERMINING THE NUMBER OF TURNS OF THE SMALL HELIX

Similarly, the number of turns for the small helix, $N_1$, is optimized for the highest 2-dB RHCP gain BW. To vary $N_1$, the number of steps of the small helix, $m_1$, is varied while $\theta_1$ and $n$, are maintained constant as shown in (4). After an iterative process the value $m_1 = 18$ is selected as a compromise between optimal 2-dB RHCP gain bandwidth at the range of 1.94 GHz-3.46 GHz, a maximum RHCP gain of 12.7 dB and an AR range of 0.4 dB-3 dB.

### D. SPACING BETWEEN ADJACENT TURNS OF BOTTOM HELIX

The next parameter to be optimized is the spacing between adjacent turns of the bottom helix, $S$. This spacing controls the frequency-band reconfigurability of the multi-radii antenna. According to (1), $S$ is only related to the *ratio* of unit lengths in Fig. 1; therefore, all other parameters of the antenna remain constant.

The simulated performance of the antenna versus $S$ is summarized in TABLE 4, which shows that as $S$ increases, the operating frequency band of the multi-radii helix shifts to lower frequencies, and the 2-dB gain bandwidth first increases and then decreases. Therefore, the optimal $S$ to achieve the widest 2-dB RHCP gain bandwidth is 31.3mm, which corresponds to a *ratio* of 0.7.

### E. SPACING BETWEEN ADJACENT TURNS OF TOP HELIX

Similarly, using (2), $S_1$ is optimized by varying $ratio_1$ and keeping all the other parameters constant. The antenna

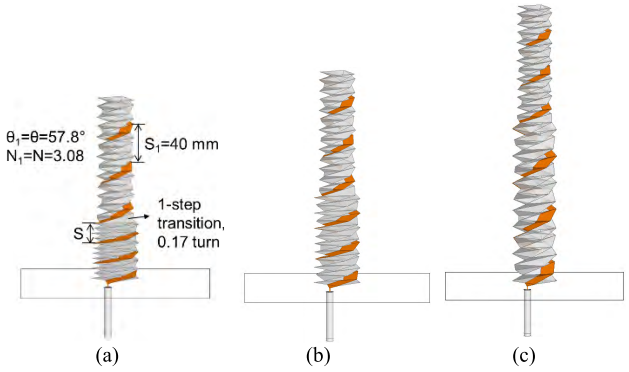


**FIGURE 4.** Models of multi-radii helix with variable $S$. (a) $S = 20$ *mm*. (b) $S = 31.3$ *mm*. (c) $S = 60$ *mm*.

**TABLE 4.** Simulated antenna performances vs pitch.

| $S$ | *ratio* | Bandwidth with -2 dB RHCP Gain Variation from the Maximum | Max. RHCP Gain | AR Range |
|---|---|---|---|---|
| 20 *mm* | 0.69 | 2.48 GHz-3.66 GHz (Δf=38.4%) | 13.9 dB | 0.2 dB-1.9 dB |
| 31.3 *mm* | 0.7 | 2 GHz-3.52 GHz (Δf=55.1%) | 13.2 dB | 0 dB-2.1 dB |
| 60 *mm* | 0.74 | 1.76 GHz-2.12 GHz (Δf=18.6%) | 9.8 dB | 0.7 dB-2.6 dB |

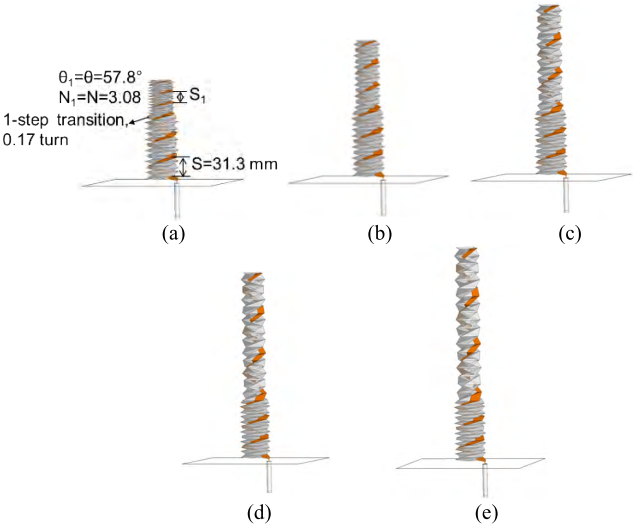


**FIGURE 5.** Models of multi-radii helix with variable $S_1$. (a) $S_1 = 16$ *mm*. (b) $S_1 = 32$ *mm*. (c) $S_1 = 50$ *mm*. (d) $S_1 = 65.6$ *mm*. (e) $S_1 = 75.2$ *mm*.

models for different values of $S_1$ are shown in Fig. 5, while in TABLE 5 the antenna performance is tabulated for the corresponding cases.

It is interesting the fact that the spacing between the adjacent turns of the top helix doesn't affect significantly the maximum RHCP gain but only the 2-dB RHCP gain bandwidth. The best value is achieved for $S_1 = 65.6$ mm.

## V. SUMMARY OF PERFORMANCE TRENDS FOR A MULTI-RADII HELICAL ANTENNA

The most critical parameters for the design of the multi-radii helical antenna are the circumferences of both helices. The circumference of the bottom helix determines the operational bandwidth, while the circumference of the top helix

**TABLE 5. Simulated antenna performances vs $S_1$.**

| $S_1$ | $ratio_1$ | Bandwidth with -2 dB RHCP Gain Variation from the Maximum | Max. RHCP Gain | AR Range |
|---|---|---|---|---|
| 16 *mm* | 0.69 | 2.4 GHz-3.1 GHz (Δf=25.5%) | 12.5 dB | 0.6 dB-3 dB |
| 32 *mm* | 0.71 | 1.96 GHz-3.48 GHz (Δf=55.9%) | 13.2 dB | 0.5 dB-2.9 dB |
| 50 *mm* | 0.75 | 1.96 GHz-3.44 GHz (Δf=54.8%) | 13.2 dB | 0.1 dB-1.2 dB |
| 65.6 *mm* | 0.79 | 1.72 GHz-3.52 GHz (Δf=68.7%) | 12.5 dB | 0.1 dB-1.4 dB |
| 75.2 *mm* | 0.82 | 1.74 GHz-3.48 GHz (Δf=66.7%) | 12.6 dB | 0.2 dB-1 dB |

improves the AR and the RHCP gain. When the circumference of the top helix, $C_1$, increases while staying smaller than $C$, the RHCP gain and AR are improved without impacting the 2-dB RHCP realized gain bandwidth. However, when $C_1$ increases beyond $C$, the RHCP gain stops increasing, and the bandwidth and AR deteriorate. When the number of turns of either the bottom or the top helix increases, the RHCP realized gain increases inside its 2-dB RHCP realized gain bandwidth, while the RHCP gain bandwidth first increases and then decreases. When the pitch size of the top helix, $S_1$, increases, the 2-dB RHCP realized gain bandwidth first increases and then decreases without significantly affecting the RHCP realized gain, and AR tends to improve. Adding a third smaller helical section on top of the multi-radii helix does not improve the bandwidth (the results for an antenna with three helices are omitted for reasons of brevity).

Based on these findings, the design process of a multi-radii helix is as follows:

1. the circumference of the bottom helix, $C$, is chosen for the desired operating frequency band based on (7);
2. the circumference of the top helix, $C_1$, is chosen to improve AR and RHCP gain in the designed frequency band, based on (7);
3. the number of turns for the bottom helix is chosen to optimize the 2-dB RHCP realized gain bandwidth using (1);
4. the number of turns for the top helix is chosen to achieve a compromise between 2-dB RHCP realized gain bandwidth and the maximum zenithal RHCP gain using (2);
5. the pitch size of the bottom helix, $S$, is chosen based on (8) and (9) and is optimized to achieve multiband operation;
6. the pitch size of the top helix, $S_1$, is chosen based on (8) and (9) and is optimized for each reconfigurable state to improve their 2-dB RHCP realized gain bandwidth and CP performance.

## VI. COMPARISON OF ORIGAMI MULTI-RADII HELIX WITH STANDARD AND ORIGAMI HELICES

### A. COMPARISON OF ORIGAMI MULTI-RADII HELIX WITH STANDARD HELIX

The performance of the semi-folded state of the origami multi-radii helix, shown in Fig. 2(b), is compared with the

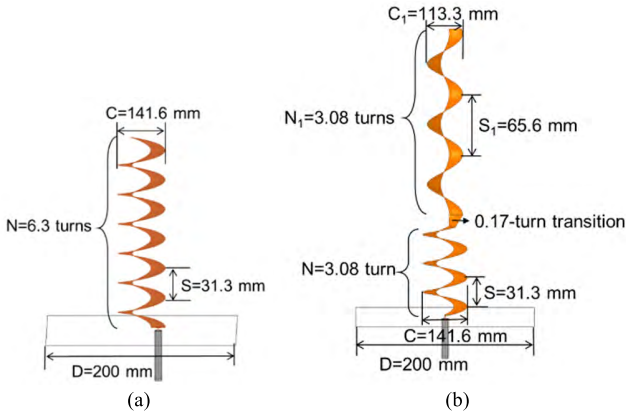


**FIGURE 6. The geometries of: (a) standard helix, and (b) standard multi-radii helix.**

performance of a standard helix and a standard multi-radii helix (see Fig. 6). The pitch sizes, circumferences, and pitch angles of the standard multi-radii helix are the same with the ones of the proposed origami multi-radii helix. Also, the geometric parameters of the standard helix are the same with the ones of the bottom helix in the origami multi-radii antenna. All three antennas have the same uniform copper width of 15 *mm* and a total number of turns of approximately 6.3. All other geometric parameters are also kept the same, including ground plane sizes ($D = 200$ *mm*), distances from the ground (3.5 *mm*), SMA feeding ports and positions of the antennas for a fair comparison. The pitch angle for all three antennas, $\alpha$, is 12.5° which falls into the optimum range (12° to 14°) to achieve optimal circular polarization [1].

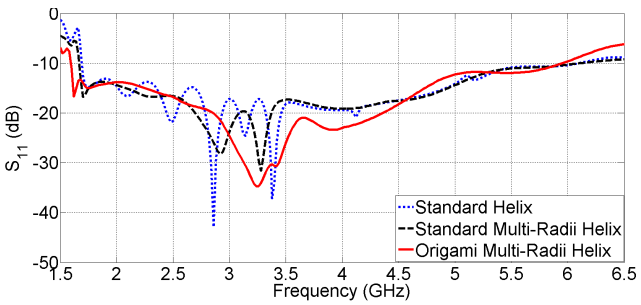


**FIGURE 7. Comparison of simulated $S_{11}$ of standard, standard multi-radii, and origami multi-radii helices.**

Figs. 7-10 compare the performance (i.e., reflection coefficient, zenithal realized RHCP gain, zenithal AR and radiation patterns) of the three antennas. In TABLE 6, the performance of the three antennas is summarized and the best performance is shaded. The simulation analysis was performed by ANSYS HFSS. The fractional bandwidth $\Delta f$ is calculated as [19]:

$$\Delta f = \frac{f_{\max} - f_{\min}}{(f_{\max} + f_{\min})/2} \times 100\% \tag{10}$$

It can be concluded from these results that:

1. The origami multi-radii helix exhibits the widest $S_{11}$ bandwidth (Fig. 7).

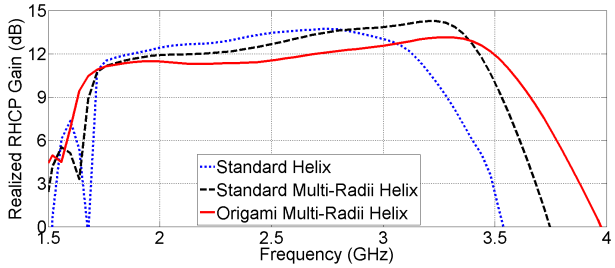


**FIGURE 8.** Comparison of simulated zenithal RHCP realized gain of standard, standard multi-radii, and origami multi-radii helices.

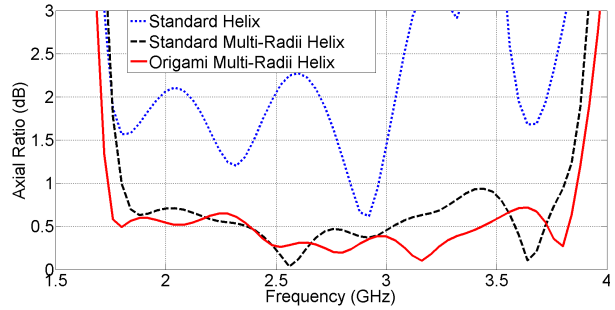


**FIGURE 9.** Comparison of simulated zenithal axial ratio of standard, standard multi-radii, and origami multi-radii helices.

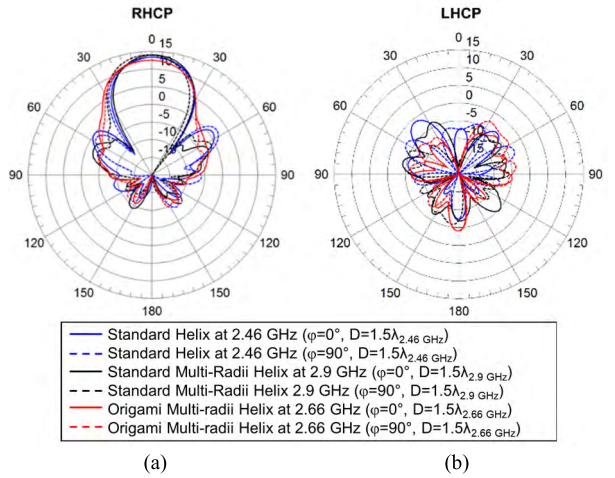


**FIGURE 10.** Comparison of simulated radiation patterns of standard, standard multi-radii, and origami multi-radii helices at their center frequency of operation, $f_c$.

2. The standard multi-radii helix has the largest RHCP realized gain but has the narrowest 2-dB RHCP realized gain bandwidth ($\Delta f = 35.9\%$).
3. The origami multi-radii helix has the widest 2-dB RHCP realized gain bandwidth ($\Delta f = 66.2\%$), which is approximately two times larger than the one of the standard multi-radii helix, while its maximum RHCP realized gain is smaller than the one of the standard multi-radii helix only by 1.1 dB (Fig. 8).
4. The origami multi-radii helix has the widest CP bandwidth with AR<3 dB and the best AR performance (i.e., AR<0.7 dB) inside the 2-dB RHCP gain bandwidth out of all the three antennas compared here (Fig. 9).
5. The origami multi-radii helix can also reconfigure its operating frequency band by changing its height as it was demonstrated in Section III, whereas the two standard helical antennas cannot.

**TABLE 6.** Performance comparison of standard, standard multi-radii, and origami multi-radii helices.

| *Antenna Performance* | *Standard Helix* | *Standard Multi-radii Helix* | *Origami Multi-radii Helix* |
|---|---|---|---|
| *$S_{11}$ BW ($S_{11}$<-10 dB)* | 1.69 GHz-6.1 GHz (Δf=113%) | 1.67 GHz-6.12 GHz (Δf=114%) | 1.6 GHz-5.95 GHz (Δf=115%) |
| *CP BW (AR<3 dB)* | 1.72 GHz-3.12 GHz (Δf=57.9%) | 1.74 GHz-3.9 GHz (Δf=76.6%) | 1.7 GHz-3.96 GHz (Δf=79.9%) |
| *Max. RHCP Gain* | 13.7 dB | 14.3 dB | 13.2 dB |
| *BW within -2 dB RHCP Gain Variation from the Maximum* | 1.78 GHz-3.12 GHz (Δf=54.7%) | 2.38 GHz-3.42 GHz (Δf=35.9%) | 1.78 GHz-3.54 GHz (Δf=66.2%) |
| *AR Range within RHCP Gain BW* | 0.6 dB-2.3 dB | 0.04 dB-0.9 dB | 0.1 dB-0.7 dB |
| *Frequency Band Reconfigurability* | No | No | Yes |

Also, the elevation radiation patterns of the three antennas at their corresponding center frequencies of operation, $f_c = (f_{max} + f_{min})/2$, are compared in Fig. 10.

Square ground planes of the same electrical size (D=1.5$\lambda_c$) at their $f_c$ were used for fair comparison of their sidelobes. It can be seen from Fig. 10 that the multi-radii helices (origami and standard) have lower sidelobes than the ones of the standard helix. Therefore, compared to the standard helices, the proposed origami multi-radii helix exhibits a 2% larger $S_{11}$ bandwidth, a 22% larger CP bandwidth, a 30.3% larger 2-dB RHCP realized gain bandwidth and the smallest AR. These outweigh the fact that the origami multi-radii helix exhibits a smaller RHCP gain by 1.1 dB compared to the standard multi-radii helix. In fact, the gain of the origami multi-radii helix can be further enhanced by adding a reflector without impairing its CP performance.

### B. PERFORMANCE COMPARISON OF ORIGAMI MULTI-RADII HELIX WITH STANDARD SINGLE-RADIUS ORIGAMI HELIX

The geometry of the single-radius (i.e., standard) origami helix at three states is shown in Fig. 11. The pitch size, $S$, circumference, $C$, and pitch angle of the origami helix are the same with the ones of the bottom helix in the origami multi-radii helix at three states (Fig. 2). Also, both origami antennas have the same number of turns at the all three states. All other geometric parameters (i.e., *n, a, ratio, w,* $\theta$) are kept the same, including the ground plane size ($D = 200\ mm$), distance from the ground (3.5 *mm*), SMA feeding port and position of the antennas for a fair comparison.

The performance (i.e., $S_{11}$, zenithal realized RHCP gain, zenithal axial ratio and elevation radiation patterns) of the

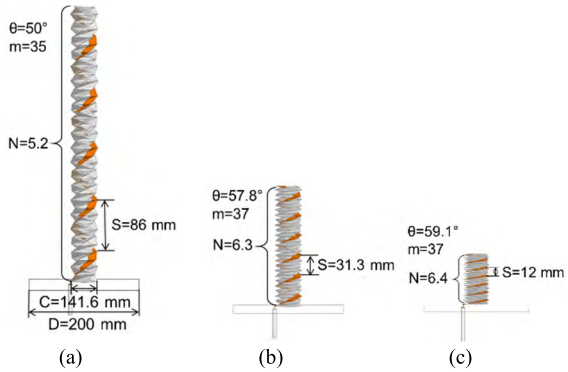


**FIGURE 11.** Standard origami helix at: (a) state 1 (unfolded state), (b) state 2 (semi-folded state), and (c) state 3 (folded state).

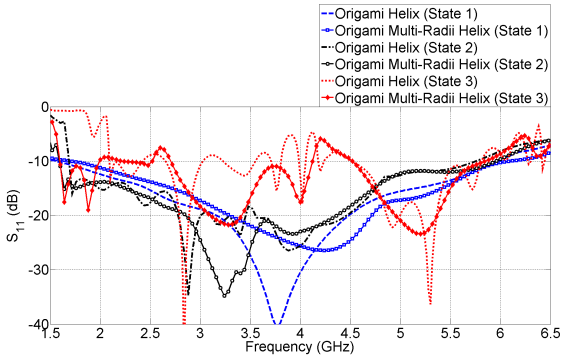


**FIGURE 12.** Comparison of simulated $S_{11}$ of origami single-radius and multi-radii helices at three states (blue lines: state 1; black lines: state 2; red lines: state 3).

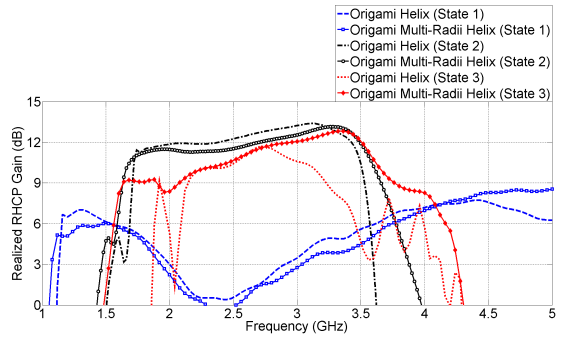


**FIGURE 13.** Comparison of simulated realized RHCP gain of origami single-radius and multi-radii helices at three states (blue lines: state 1; black lines: state 2; red lines: state 3).

origami singe-radius and multi-radii helices is compared in all three states of operation in Figs. 12-15.

The comparison of these results is summarized in TABLE 7. The following conclusions are drawn:

1. The standard origami helix (Fig. 11), can operate in only the first two states with CP performance covering the following frequency band: 1.3 GHz-1.78 GHz and 1.78 GHz-3.46 GHz. However, the proposed origami multi-radii helix can operate at three states with CP performance covering the following bands: 1.22 GHz-1.84 GHz and 1.78 GHz-3.54 GHz and 3.64 GHz-4.04 GHz, depending on the gain requirements. Especially the third state can operate in the range 3.64 GHz-4.4 GHz with a gain of 6 dB in the upper band.
2. The origami multi-radii helix has smaller maximum AR at states 2 and 3, as shown in Fig. 14.
3. At states 2 and 3, the origami multi-radii helix has lower sidelobe level than that of the standard origami helix. Also, at state 3 the origami multi-radii helix has a maximum RHCP gain that is larger by 2.8 dB than the one of the standard origami helix.

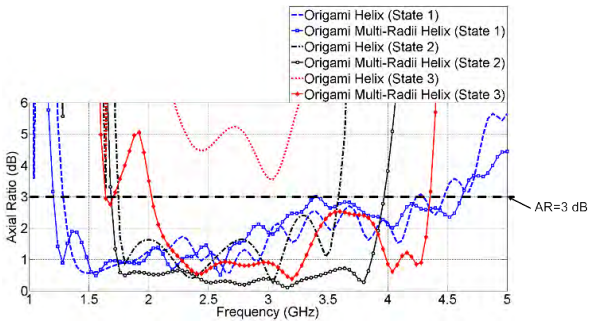


**FIGURE 14.** Comparison of simulated axial ratio of origami single-radius and multi-radii helices at three states (blue lines: state 1; black lines: state 2; red lines: state 3).

**TABLE 7.** Performance comparison of origami single-radius and multi-radii helices at three states.

| State of Origami Antennas | | $S_{11}$ BW ($S_{11}$<-10 dB) | CP BW (AR<-3 dB) | Realized RHCP Gain BW within -2 dB Variation from the Maximum | Max. Realized RHCP Gain | AR Range within 2-dB RHCP Gain BW |
|---|---|---|---|---|---|---|
| 1 | Origami Helix | 1.56 GHz-5.96 GHz (Δf=117%) | 1.32 GHz-4.2 GHz (Δf=104%) | 1.3 GHz-1.78 GHz (Δf=31.2%) | 7 dB | 0.6 dB-3 dB |
| | Origami Multi-radii Helix | 1.7 GHz-6.1 GHz (Δf=113%) | 1.22 GHz-3.4 GHz (Δf=94%) | 1.22 GHz-1.84 GHz (Δf=42.1%) | 6.1 dB | 0.5 dB-3 dB |
| 2 | Origami Helix | 1.7 GHz-5.76 GHz (Δf=109%) | 1.75 GHz-3.59 GHz (Δf=68.9%) | 1.78 GHz-3.46 GHz (Δf=64.1%) | 13.4 dB | 0.3 dB-2.4 dB |
| | Origami Multi-radii Helix | 1.6 GHz-5.96 GHz (Δf=116%) | 1.69 GHz-3.94 GHz (Δf=79.9%) | 1.78 GHz-3.54 GHz (Δf=66.2%) | 13 dB | 0.1 dB-0.6 dB |
| 3 | Origami Helix | 2.66 GHz-3.02 GHz (Δf=12.7%) | N/A | 3.9 GHz-4 GHz (Δf=2.5%) | 7.3 dB | 9 dB-10 dB |
| | Origami Multi-radii Helix | 2.18 GHz-4.1 GHz (Δf=116%) | 1.6 GHz-4.4 GHz (Δf=93.3%) | 3.64 GHz-4.04 GHz (Δf=10.4%) | 10.1 dB | 0.6 dB-2.5 dB |

Fig. 13 shows that the realized RHCP gain of the origami helices at state 1 significantly decreases in the frequency range of 2 GHz-3 GHz. This occurs because the geometrical parameters of the helical antennas do not satisfy conditions (6) and (7) in this frequency range. For example, at $f = 2.5\,GHz$ the pitch size of the bottom helix, $S$, (which mainly affects the antenna performance) is $0.7\lambda_0$ and its circumference, $C = 1.2\lambda_0$. On the contrary, at a lower frequency, e.g., $f = 1.5\,GHz$, the gain is high (i.e., 6 dB) because the pitch size, $S$ is $0.4\lambda_0$ and the circumference $C = 0.71\lambda_0$, which are much closer to the optimal values provided by (6) and (7). Also, at state 1, the origami helices operate efficiently at frequencies higher than 2.5 GHz because they

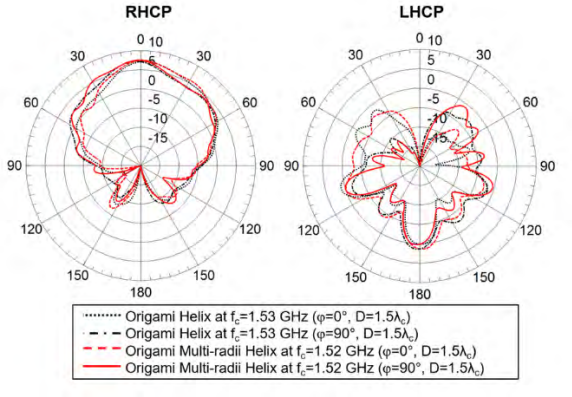


(a) State 1 at $f_c$

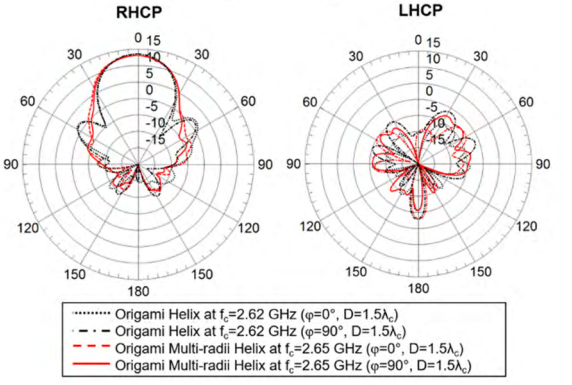


(b) State 2 at $f_c$

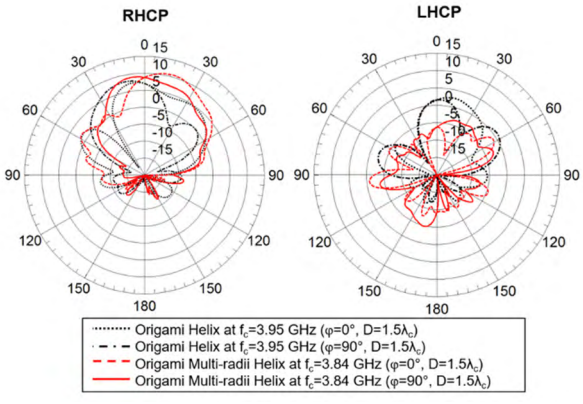


(c) State 3 at $f$

**FIGURE 15.** Comparison of simulated elevation radiation patterns of the origami single-radius and multi-radii helices at the center frequencies $f_c$ in their 2-dB realized gain bandwidths at: (a) state 1; (b) state 2; and (c) state 3.

resonate at a higher-order mode. This can be easily validated by seeing that at a higher frequency, such as $f = 4\ GHz$ the pitch size, $S = \lambda_0$ and the circumference, $C = 1.8\lambda_0$, which confirm that the helices operate at a higher-order mode indeed [10], [13, p. 230]. A general observation that can be done is about the maximum gain variation along the frequency. Figs. 12-14 show that at each state the multi-radii helical antenna operates efficiently at a different frequency band. This behavior is expected (supportive results were also shown in [18]) and it can be attributed to the change of the

(a) (b) (c)

**FIGURE 16.** Prototype of origami multi-radii helix at 3 reconfigurable states. (a) State 1. (b) State 2. (c) State 3.

**TABLE 8.** Dimensions of actuation mechanism.

| *H* | *H1* | *a* | *a1* | *r* | *r1* |
|---|---|---|---|---|---|
| 232 *mm* | 552 *mm* | 35.3 *mm* | 28 *mm* | 4.5 *mm* | 2.6 *mm* |

electrical characteristics of the antenna along the frequency. The performance of a helical antenna (e.g., gain, bandwidth of operation, axial ratio) depends on its geometrical parameters [10], such as the pitch angle, the spacing between the turns, the diameter of the helix, the length of one turn, etc. In the case of a physically reconfigurable structure, such as our origami helix, several of its geometrical parameters change (e.g., distance between the turns, total height of the structure, etc.) at the different states and in turn provide different performance.

## VII. FABRICATION OF ANTENNA AND ACTUATION MECHANISM

### A. FABRICATION OF THE ORIGAMI MULTI-RADII HELIX

The origami base of the designed origami multi-radii helix in Fig. 2 is fabricated using 2-mil thick FPC Kapton, which is a material used for space applications. An axial force, applied on the top step of the antenna, is needed to deploy and stow the antenna. As the antenna collapses it also rotates. The rotated angle between the two states is: $m\cdot\Delta\theta+(1+m_1)\cdot\Delta\theta_1$. The 2-mil thick FPC Kapton is more suitable than a thicker substrate, since it requires less force to change the antenna height and maintains the shape of the folded planes without deformation. Also, this antenna can collapse to be stowed in a compact volume given by [2],

$$Volume_{compact} = \frac{(m + m_1 + 1)tn^2a^2}{\pi} \tag{11}$$

where $t$ is the thickness of flexible substrate, the footprint of the origami base is $n^2a^2/(4\pi)$, and the height of the compacted origami base is $4(m + m_1 + 1)t$. The folding pattern in Fig. 1 is perforated with Silhouette Cameo on the Kapton substrate for accurate creases. A 3-mil copper trace is glued on the 2-mil planar FPC Kapton substrate as shown in Fig. 1 and then the 3-D antenna is folded up, as shown

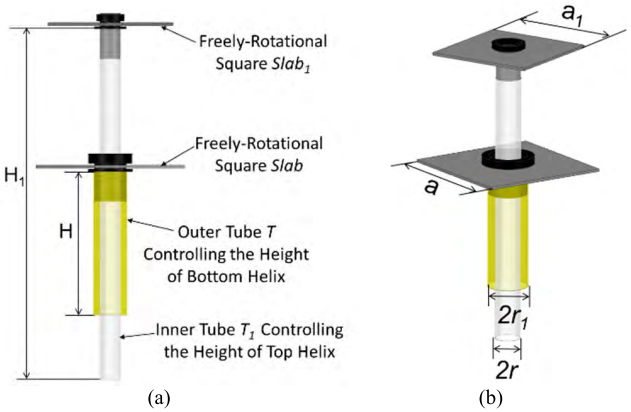


**FIGURE 17.** Actuation mechanism of the origami multi-radii helix. (a) Side view. (b) Perspective view.

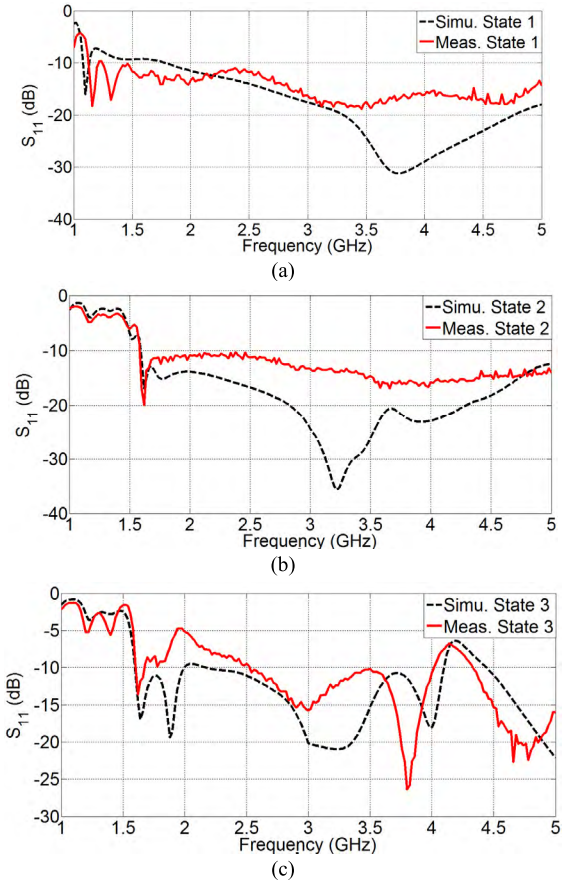


**FIGURE 18.** Simulated and measured $S_{11}$ results of the origami multi-radii helix at: (a) state 1, (b) state 2 and (c) state 3.

in Fig. 16. The ground plane is built using a 1-mm thick FR4 board that is metallized on one side. It is important to note that the proposed antenna, when it is stowed, occupies approximately 29.5 times smaller volume versus when it is fully deployed. The volume savings for this antenna can be calculated as:

$$\frac{Volume_{compact}}{Volume_{unfolded}} = \frac{4(m+m_1+1)t}{S \cdot N + S_1 \cdot (N_0+N_1)} \tag{12}$$

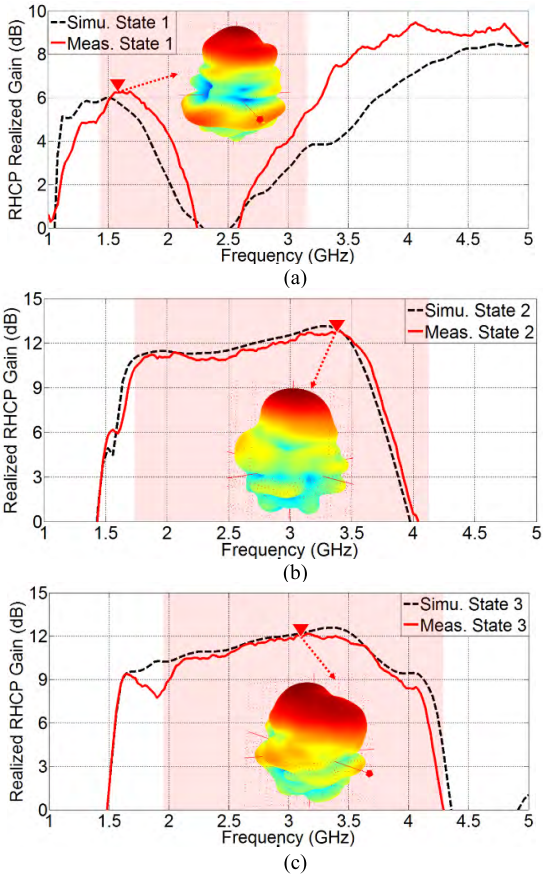


**FIGURE 19.** Simulated and measured realized RHCP gain of the origami multi-radii helix at: (a) state 1, (b) state 2 and (c) state 3.

### B. ACTUATION MECHANISM

An actuation mechanism is proposed for this antenna as shown in Fig. 17 that can reconfigure the antenna height without the need of a rotation mechanism. This actuation mechanism is placed along the axis of the helical antenna. Two free-to-rotate 1 mm-thick square slabs are positioned at the top end of two concentric tubes, as shown in Fig. 17(a). The larger square *Slab* is fixed to the 4 sides of the top of the bottom origami cylinder base, and the smaller square $Slab_1$ is fixed to the 4 sides of the top of the top origami cylinder base.

The bottom ends of the two concentric tubes $T$ and $T_1$ are movable. After installing the antenna on its ground plane, $T$ is used to adjust the height of the bottom helix $H$, then $T_1$ is used to adjust the height of the top helix ($H_1$-$H$). The concentric tubes are 0.15-mm thin polypropylene, so its dielectric property does not affect the antenna performance. Also, the polypropylene tubes are bendable to accommodate antenna measurement in the anechoic chamber. The other parts of the actuation mechanism are made of PLA and are 3-D printed. Since these PLA parts are electrically small ($<0.045\lambda$), they also have little impact on the antenna performance. The main dimensions of the actuation mechanism are listed in TABLE 8.

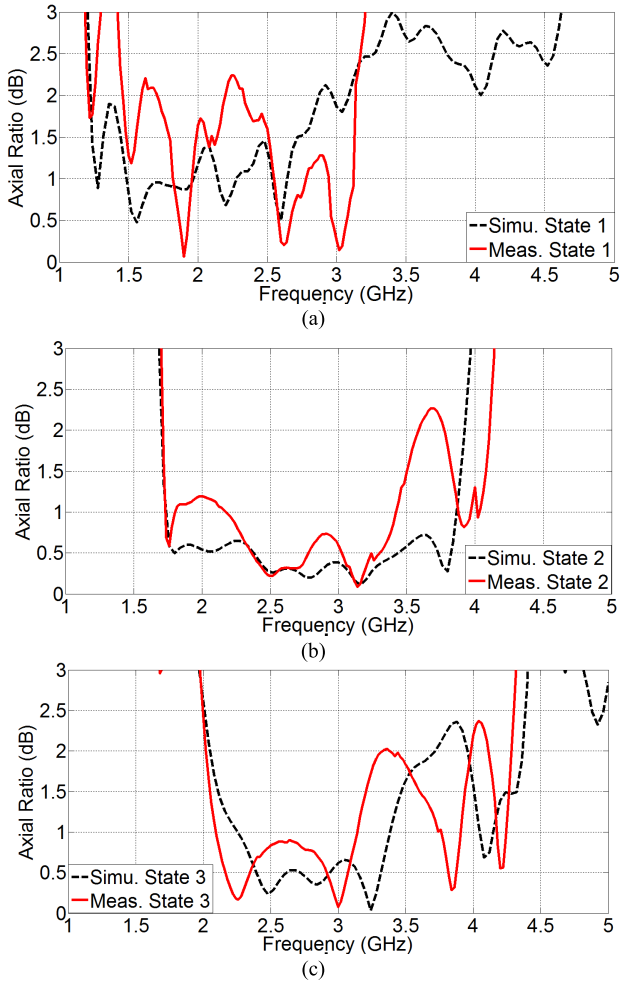


**FIGURE 20.** Simulated and measured axial ratio of the origami multi-radii helix at: (a) state 1, (b) state 2 and (c) state 3.

## VIII. SIMULATED AND MEASURED RESULTS

The wideband frequency reconfigurability of the proposed origami multi-radii helix is validated with simulated and measured results, as shown in Fig. 18-21 and TABLE 9. In Fig. 19 the measured 3-D pattern at the operating frequency with maximum RHCP gain of each state is shown, and the CP bandwidth where the AR is less than 3 dB is shaded. The severe decrease of the gain at state 1 in the frequency range 2 GHz-3GHz, is caused by the geometrical parameters of the antenna not satisfying conditions (6) and (7) (this was explained in detail in Section VI-B). Even though this dip in gain seems undesired at a first glance, it can be very useful in some cases. Countries, which are using parts of the band 2300-2700 MHz for BSS (Broadcasting Satellite Services), MSS (Mobile Satellite Services) or FSS (Fixed Satellite Service) networks, demand geographical separation of the services or band segmentation to avoid spurious and out-of-band emissions. Therefore, the decrease in gain, which the origami helices experience at certain frequencies in state 1, can be used to effectively filter RF signals at these frequencies without requiring additional filters in the RF front-ends of these helices. Fig. 21 shows the radiation patterns at these

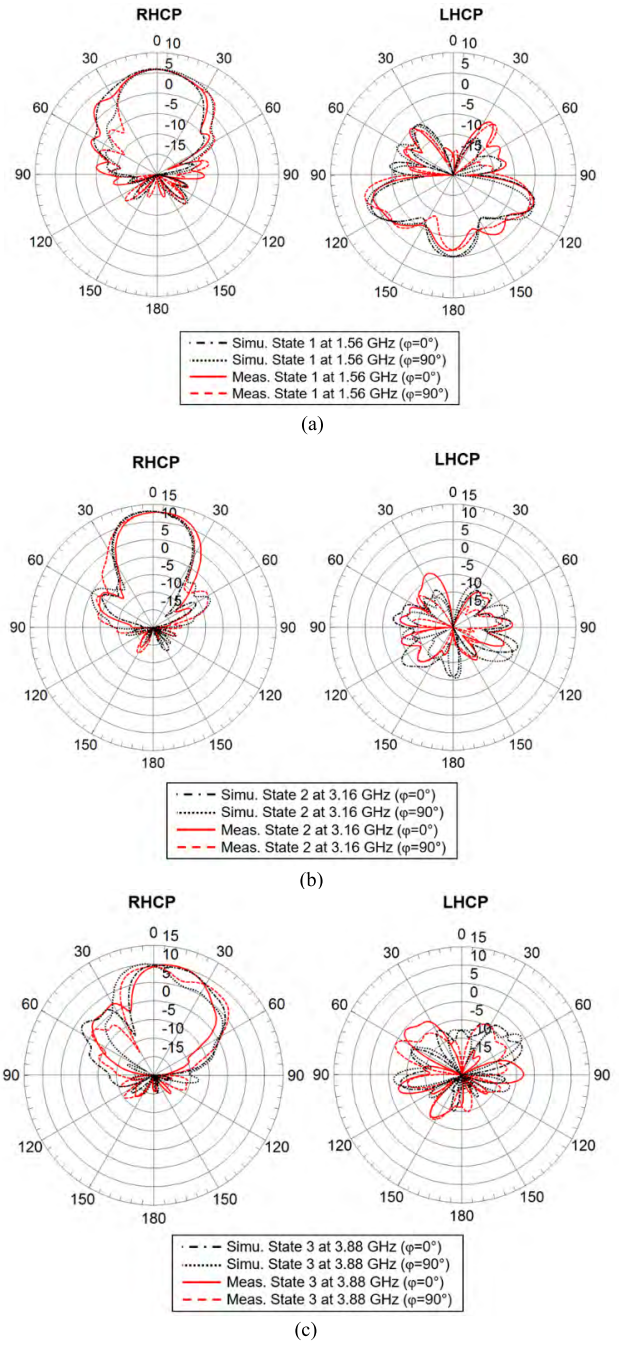


**FIGURE 21.** Simulated and measured elevation radiation patterns of the origami multi-radii helix at: (a) state 1 at 1.56 GHz, (b) state 2 at 3.16 GHz, and (c) state 3 at 3.88 GHz.

typical operating frequencies. All the measurements were performed using a StarLab Anechoic Chamber.

Our measured results validate that our origami multi-radii helix can change its height to reconfigure its operation between 3 states while maintaining RHCP. Specifically, this design is capable for GPS, Satellite Radio and WiMAX applications. As it is shown in Table 9, state 1 is suitable for the low band of 1.42 GHz-2.01 GHz covering the GPS band (1.575 GHz) with a gain of 6.1 dB and an AR below 1.5 dB.

**TABLE 9. Simulated and measured results of the origami multi-radii helix at 3 states.**

| State of Origami Antennas | | CP BW (AR<-3 dB) | Realized RHCP Gain BW within -2 dB Variation from the Maximum | Max. Realized RHCP Gain | AR Range within 2-dB RHCP Gain BW |
|---|---|---|---|---|---|
| 1 | Simu. | 1.22 GHz-3.4 GHz (Δf=94%) | 1.22 GHz-1.84 GHz (Δf=42.1%) | 6.1 dB | 0.5 dB-3 dB |
| | Meas. | 1.42 GHz-3.2GHz (Δf=77.1%) | 1.42 GHz-2.01 GHz (Δf=34.4%) | 6.3 dB | 0.1 dB-3 dB |
| 2 | Simu. | 1.69 GHz-3.94 GHz (Δf=79.9%) | 1.78 GHz-3.54 GHz (Δf=66.2%) | 13 dB | 0.1 dB-0.6 dB |
| | Meas. | 1.7 GHz-4.14 GHz (Δf=83.6%) | 1.78 GHz-3.64 GHz (Δf=68.6%) | 12.7 dB | 0.1 dB-2.2 dB |
| 3 | Simu. | 1.6 GHz-4.4 GHz (Δf=93.3%) | 3.64 GHz-4.04 GHz (Δf=10.4%) | 10.1 dB | 0.6 dB-2.5 dB |
| | Meas. | 1.98 GHz-4.3 GHz (Δf=73.9%) | 3.72 GHz-4.06 GHz (Δf=8.7%) | 10.5 dB | 0.3 dB-2.4 dB |

Also, according to Table 9, states 2 or 3 can cover WiMAX and Satellite Radio, respectively, since each one state exhibits higher gain in its respective application. Especially for downlink C-band services (e.g., 3700-4200 MHz in USA, 3625-4200 MHz in Brazil), the state 3 is the most suitable one than all three antenna states, as it provides a realized RHCP gain of 6 dB. Even higher gains can be achieved by increasing the size of the ground plane as shown in [22].

## IX. CONCLUSIONS

This paper presents the design of a physically reconfigurable multi-radii antenna that can be stowed efficiently. The volume of this antenna at its stowed state is approximately 29.5 times smaller than its volume when it is fully deployed. Also, this antenna can dynamically change its height to reconfigure its performance and operate in different bands while maintaining circular polarization for applications, such as, GPS, satellite radio, WiMax and satellite communications. The performance of this antenna was validated through simulations and measurements. The design process for this antenna along with its optimization were also provided. In addition, this antenna outperforms the standard single and multi-radii helical antennas as it exhibits larger bandwidths. Finally, the current design outperforms the single-radius origami helix as it exhibits improved CP performance at all three states of operation.

## REFERENCES

[1] S. Yao, X. Liu, and S. V. Georgakopoulos, "Morphing origami conical spiral antenna based on the Nojima wrap," *IEEE Trans. Antennas Propag.*, vol. 65, no. 5, pp. 2222–2232, May 2017.

[2] X. Liu, S. Yao, B. S. Cook, M. M. Tentzeris, and S. V. Georgakopoulos, "An origami reconfigurable axial-mode bifilar helical antenna," *IEEE Trans. Antennas Propag.*, vol. 63, no. 12, pp. 5897–5903, Dec. 2015.

[3] J. Costantine *et al.*, "UHF deployable helical antennas for CubeSats," *IEEE Trans. Antennas Propag.*, vol. 64, no. 9, pp. 3752–3759, Sep. 2016.

[4] A. J. Ernest, Y. Tawk, J. Costantine, and C. G. Christodoulou, "A bottom fed deployable conical log spiral antenna design for CubeSat," *IEEE Trans. Antennas Propag.*, vol. 63, no. 1, pp. 41–47, Jan. 2015.

[5] X. Bai, J. Tang, X. Liang, J. Geng, and R. Jin, "Compact design of triple-band circularly polarized quadrifilar helix antennas," *IEEE Antennas Wireless Propag. Lett.*, vol. 13, pp. 380–383, 2014.

[6] S. I. H. Shah, M. M. Tentzeris, and S. Lim, "Low-cost circularly polarized origami antenna," *IEEE Antennas Wireless Propag. Lett.*, vol. 16, pp. 2026–2029, Apr. 2017.

[7] W. Su, R. Bahr, S. A. Nauroze, and M. M. Tentzeris, "3D printed reconfigurable helical antenna based on microfluidics and liquid metal alloy," in *Proc. IEEE Int. Symp. Antennas Propag. (APSURSI)*, Fajardo, Puerto Rico, Jun./Jul. 2016, pp. 469–470.

[8] S. Yao and S. V. Georgakopoulos, "Origami segmented helical antenna with switchable sense of polarization," *IEEE Access*, vol. 6, pp. 4528–4536, Dec. 2017.

[9] X. Liu, S. V. Georgakopoulos and S. Rao, "A design of an origami reconfigurable QHA with a foldable reflector," *IEEE Antennas Propag. Mag.*, vol. 59, no. 4, pp. 78–105, Aug. 2017.

[10] J. D. Kraus, "The helical antenna," *Proc. IRE*, vol. 37, no. 3, pp. 263–272, Mar. 1949.

[11] J. D. Kraus, "Helical beam antennas for wide-band applications," *Proc. IRE*, vol. 36, no. 10, pp. 1236–1242, Oct. 1948.

[12] J. D. Kraus, "Characteristics of helical antennas radiating in the axial mode," *J. Appl. Phys.*, vol. 19, pp. 87–98, Jan. 1948.

[13] J. D. Kraus and R. J. Marhefka, *Antennas For All Applications*, 3rd ed. New York, NY, USA: McGraw-Hill, 2003.

[14] H. Barsky, "Broadband conical helix antennas," in *Proc. IRE Int. Conv. Rec.*, New York, NY, USA, 1959, pp. 138–146.

[15] P. W. Klock, "A study of wave propagation of helices," Elect. Eng. Res. Lab., Univ. Illinois Urbana, Antenna Lab., Champaign, IL, USA, Tech. Rep. 68, Mar. 1963.

[16] J. S. Chatterjee, "Helical log-periodic array," *IEEE Trans. Antennas Propag.*, vol. AP-16, no. 5, pp. 592–593, Sep. 1968.

[17] D. Y. Stephenson and P. E. Mayes, "Broadband arrays of helical dipoles," Elect. Eng. Res. Lab., Univ. Illinois Urbana, Antenna Lab., Champaign, IL, USA, Tech. Rep. 2, Jan. 1964.

[18] J. L. Wong and H. E. King, "Broadband quasi-taper helical antennas," *IEEE Trans. Antennas Propag.*, vol. AP-27, no. 1, pp. 72–78, Jan. 1979.

[19] C. Balanis, *Antenna Theory and Design*, 3rd ed. Hoboken, MA, USA: Wiley, 2012, pp. 217–219.

[20] C. Jiangguo, D. Xiaowei, Z. Ya, F. Jian, and T. Yongming, "Bistable behavior of the cylindrical origami structure with Kresling pattern," *J. Mech. Des.*, vol. 137, pp. 061406-1–061406-8, Jun. 2015.

[21] C. Lv, "Theoretical and finite element analysis of origami and kirigami based structures," Ph.D. dissertation, Dept. Mech. Eng., Arizona State Univ., Tempe, AZ, USA, Aug. 2016.

[22] A. R. Djordjevic, A. G. Zajic, and M. M. Ilic, "Enhancing the gain of helical antennas by shaping the ground conductor," *IEEE Antennas Wireless Propag. Lett.*, vol. 5, no. 1, pp. 138–140, Dec. 2006.

[23] Y. Zhinong, "Multi-band non-uniform helical antennas," U.S. Patent 6 112 102, Aug. 29, 2000.

**XUELI LIU** was born in Yinchuan, China, in 1987. She received the B.S. degree in applied physics and the M.S. degree in electromagnetic field and microwave technology from the University of Electronic Science and Technology of China, Chengdu, Sichuan, China, in 2009 and 2012, respectively, and the Ph.D. degree in electrical engineering from Florida International University (FIU), Miami, FL, USA, in 2018.

From 2012 to 2013, she was a Teaching Assistant with Baylor University. From 2013 to 2018, she was a Research Assistant with the Electromagnetic Laboratory, FIU. In 2018, she was a Postdoctoral Fellow with the Transforming Antennas Center, FIU. Her research interests include frequency multipliers, optical grating, and origami antennas.

**CONSTANTINOS L. ZEKIOS** (S'03–M'15) received the Diploma degree (Hons.) in electrical and computer engineering, the M.S. degree (Hons.) in electrical and computer engineering communication and satellite telecommunication systems, and the Ph.D. degree (Hons.) in electrical and computer engineering from the Democritus University of Thrace, Xanthi, Greece, in 2008, 2011, and 2015, respectively. From 2016 to 2018, he was a Postdoctoral Researcher with the Electrical and Computer Engineering Department, University of Massachusetts Amherst, Amherst, MA, USA. He is currently a Fellow Post-Doctoral Researcher with the Electromagnetic Laboratory, Florida International University. His main research interests include microwave engineering, computational electromagnetics, and antennas.

**STAVROS V. GEORGAKOPOULOS** (S'93–M'02–SM'11) received the Diploma degree from the University of Patras, Patras, Greece, in 1996, and the M.S. and Ph.D. degrees from Arizona State University, Tempe, AZ, USA, in 1998 and 2001, respectively, all in electrical engineering. From 2001 to 2007, he was a Principal Engineer with SV Microwave, Inc. Since 2007, he has been with the Department of Electrical and Computer Engineering, Florida International University, Miami, FL, USA, where he is currently a Professor and the Director of the Transforming Antennas Center (a research center on foldable/origami, physically reconfigurable, and deployable antennas) and the RF Communications, Millimeter-Waves, and Terahertz Laboratory.

His current research interests include novel antennas/arrays, RFID, microwave and RF systems, novel sensors and wireless powering of portable, and wearable and implantable devices. He received the 2015 FIU President's Council Worlds Ahead Faculty Award, which is the highest honor, FIU extends to a faculty member for excelling in research, teaching, mentorship, and service. Since 2013, he has been serving as an Associate Editor for the IEEE TRANSACTIONS ON ANTENNAS AND PROPAGATION.